Desalination and Water Treatment
www.deswater.com
doi: 10.1080/19443994.2015.1030780

57 (2016) 9531–9548
May

Taylor & Francis
Taylor & Francis Group

Sensitivity and uncertainty analysis of an integrated membrane bioreactor model

Giorgio Mannina, Alida Cosenza*, Gaspare Viviani

Dipartimento di Ingegneria Civile, Ambientale, Aerospaziale, dei Materiali—Università di Palermo, Viale delle Scienze, 90128 Palermo, Italy, email: Giorgio.mannina@unipa.it (G. Mannina), Tel. +39 23896514; Fax: +39 091 23860810; email: alida.cosenza@unipa.it (A. Cosenza), email: gaspare.viviani@unipa.it (G. Viviani)

Received 22 December 2014; Accepted 11 March 2015

ABSTRACT

Sensitivity and uncertainty analysis, although can be of primarily importance in mathematical modelling approaches, are scarcely applied in the field of membrane bioreactor (MBR). An integrated mathematical model for MBR is applied with the final aim to pin down sources of uncertainty in MBR modelling. The uncertainty analysis has been performed combining global sensitivity analysis (GSA) with the generalized likelihood uncertainty estimation (GLUE). The model and methodology were applied to a University Cape Town pilot plant. Results show that the complexity of the modelled processes and the propagation effect from the influent to the effluent increase the uncertainty of the model prediction. It was found that the uncertainty of nitrogen and phosphorus model outputs increases from the first reactor-section plant to the last. Results show also that the GSA-GLUE methodology is a valid tool for uncertainty assessment for MBR modelling. Furthermore, the GSA-GLUE allows to identify the most critical processes/plant sections and the key sources of uncertainty where attention should be paid in view of model predictions improvement.

Keywords: Uncertainty analysis; Wastewater modelling; Global sensitivity analysis; Membrane bioreactors

1. Introduction

In the last decade, the use of membrane bioreactor (MBR) technology for treating municipal wastewater has increased considerably [1]. Despite such an interest, the knowledge related to some processes is not complete and is in need of further studies. In this context, mathematical modelling of MBR plays an important role as useful support for "MBR knowledge upgrading". In the technical literature, several MBR models have been proposed in literature adapting or integrating the activated sludge models (ASMs) originally developed for conventional activated systems [2–4].

In order to simulate the MBR systems, the original form of the ASMs has been widely modified [3]. In particular, three main types of MBR models have been developed so far [3]: hybrid models, physical models and integrated models. The hybrid models are derived by the ASMs slightly modifying the model equations to include the soluble microbial products (SMPs) which are of relevance for MBRs. Indeed, several

*Corresponding author.

authors have demonstrated that SMPs promote membrane fouling reducing membrane permeability (among others, Ahmed et al. [5]). Physical models describe only MBR physical separation processes and are generally based on the resistance in series models [3]. Finally, the integrated models couple hybrid models with physical models and represent the most powerful tool for simulating MBR systems [6,7]. Indeed, the integrated models, taking into account physical and biological processes, provide the right interpretation of MBR systems [4,8]. Recently, Zuthi et al. [7] have underlined the importance of using integrated modelling approach to better simulate membrane fouling. Thus, by adopting integrated models, the modeller may have the opportunity to improve the performance of her/his predictions by understanding the system in a comprehensive way (considering both biological and physical processes simultaneously). However, although the application of integrated MBR models can represent an useful tool for MBR design and operation, only few integrated models have been developed so far [4,8–10]. Furthermore, the model structure is generally complex and constitutes a critical issue faced by modellers. Moreover, owning to data and knowledge lacking, a considerable number of assumptions on model structure, model parameter values and input variables are generally made [11–13]. Such assumptions and the intrinsic uncertainty of biological processes can make model predictions extremely uncertain. In this context, sensitivity and uncertainty analysis can be of use for both modellers and practitioners dealing with MBR. Indeed, by means of sensitivity analysis, the modeller may identify the main factors affecting model response. On the other hand, uncertainty analysis enables to identify the effectiveness of model predictions by propagating, via the model, all model factors or structural uncertainties [14]. Therefore, uncertainty analysis can play an important key role in MBR modelling. As a matter of a fact, insight gained from uncertainty and sensitivity analysis can be of use to cope with the lack of knowledge in the interpretation of some involved phenomena (e.g. phosphorus uptake and release mechanisms and/or membrane fouling etc.). During the recent years, in the field of wastewater modelling, models' uncertainty issue has had an increasing interest among researchers. However, in the MBR wastewater field, only few studies have been carried out compared to other research field such as hydrology [15,16]. Recently, uncertainty methodologies, previously used in other research fields (e.g. hydrology), have been investigated and compared in order to discuss their applicability to wastewater treatment plant (WWTP) models. Recently, several authors have demonstrated the ability of global sensitivity analysis (GSA) to quantify uncertainties [17–19]. Similarly, the applicability of the generalized likelihood uncertainty estimation (GLUE) proposed by Beven and Binley [20], most widely used for investigating uncertainty in hydrology, has been discussed in the wastewater field [21]. The GLUE method is a sensitivity method (Monte Carlo Filtering, Hornberger-Spear-Yong (HSY), regional sensitivity analysis) combined with an error propagation of the "behavioural" models.

On the other hand, the combination of GSA and GLUE, formerly proposed by Ratto et al. [22] and recently applied in the urban drainage field [23], can be a powerful tool for improving MBR modelling results. Indeed, the GSA-GLUE approach has two main advantages: (1) provides a quantitative assessment of model factors which influence the behavioural model runs by means of GSA; (2) allows to take into account the performance of the GSA conditioned to the observations. However, as far as authors are aware, no applications of the GSA-GLUE approach to the wastewater modelling field exist.

Bearing in mind the considerations discussed above, the aim of the study is twofold: identify the model factors which contribute significantly to the uncertainty of an integrated MBR model and assess the feature of the GSA-GLUE in the wastewater modelling field. To accomplish such a goal, the GSA-GLUE has been applied to an integrated ASM2d—soluble microbial product—(ASM2d-SMP) model, developed in previous studies, applied to a University Cape Town (UCT) MBR pilot plant.

2. Materials and methods

2.1. Model description and case study

The mathematical model is an integrated MBR model that takes into account both physical (fouling prediction) and biological processes (including nutrient removal), coupled with the SMP formation/degradation processes. In particular, the integrated MBR model is able to simulate the phosphorus removal process, often neglected in the modelling literature [7]. The model was developed during previous studies [10,24]; in the following, the model structure is briefly presented.

The integrated ASM2d-SMP model is divided into two sub-models (biological and physical). The biological sub-model involves 19 biological state variables and 73 parameters (i.e. kinetics, stoichiometry and fractionation coefficients). For the variables, process

and parameter descriptions, the reader is referred to the literature [10,24]. The biological sub-model simulates the biological nutrient removal processes occurring in a UCT-MBR system and the SMPs formation/degradation. Specifically, the biological sub-model is a modified version of ASM2d [2] and includes two new variables, S_{UAP} and S_{BAP}, that, respectively, represent the soluble substrate utilisation products and the soluble biomass associated products. The sum of S_{UAP} and S_{BAP} is equal to SMP. In order to describe the SMP formation/degradation, the biological sub-models include six new processes (anaerobic, aerobic and anoxic hydrolysis of both S_{UAP} and S_{BAP}) with respect to the original AMS2d. Further, in the biological sub-model, the kinetic hydrolysis process of very slowly hydrolysable compounds (X_I) according to Lubello et al. [25] is introduced.

The physical sub-model simulates the cake layer formation on membrane surface. It is characterised by two physical state variables and six physical parameters and enables to simulate the following processes: cake layer formation during the membrane filtration; COD removal by biological membrane (i.e. cake layer); COD removal by physical membrane and the membrane resistances. The membrane is modelled by dividing its surface into equal fractions and for each fraction, the equations of Table 1 are computed. The apparent shear intensity of the fluid turbulence (G) is evaluated in accordance with the sectional approach [26]. Thus, according to the modelling approach, the fouling is not considered uniformly distributed on the membrane area surface. During the filtration phase, two opposite forces (drag and lifting) (Eqs. (1) and (2), Table 1) regulate the probability (E) of the particle being deposited on the membrane surface (Eq. (3), Table 1). The probability E, on the basis of the biomass sludge concentration (C_{SS}), influences the rates of biomass attachment onto the membrane surface (Eq. (4), Table 1). Conversely, the rate of sludge detachment is evaluated as a function of the stickiness of biomass (α), the compression coefficient for the dynamic sludge layer (γ) and the volume of permeate produced (V_f), in a fixed filtration time t (Eq. (5), Table 1). The detachment during backwashing period is described as a function of the coefficient of sludge detachment, η_c (Eq. (6), Table 1). The rate of the net cake deposition is computed as differences between the rates of biomass attachment and detachment (Eq. (7), Table 1). The concentration of the COD at the physical membrane surface (C_{sm}) is evaluated as a function of the

Table 1
Main equations of the physical sub-model

Description	Equations	Number
Drag force	$F_a = 3\pi\mu_s d_p J$	(1)
Lifting force	$F_l = C_d d_p \mu_s G \frac{\pi d_p^2}{8}$	(2)
Probability of particle deposition on membrane surface	$E = \frac{F_a}{F_l + F_a} = \frac{24J}{24J + C_d d_p G}$	(3)
Rate of biomass attachment	$\left(\frac{dM_{dc}}{dt}\right)_a = EC_{SS}J = \frac{24C_{SS}J^2}{24J + C_d d_p G}$	(4a)
Rate of sludge detachment	$\left(\frac{dM_{dc}}{dt}\right)_d = -\frac{\beta(1-\alpha)GM_{dc}^2}{\gamma V_f t + M_{dc}}$	(5)
Net cake deposition	$\frac{dM_{sc}}{dt} = \frac{24C_{SS}J^2}{24J + C_d d_p G} - \frac{\beta(1-\alpha)GM_{dc}^2}{\gamma V_f t + M_{dc}}$	(6)
Detachment rate during backwashing	$\frac{dM_{sc}}{dt} = -\eta_c M_{sc}$	(7)
Deep-bed filtration	$C_{sm} = C_S e(-\lambda\delta)$	(8)
ith total resistance	$R_{tS,i} = R_m + R_{p,i} + R_{c,i} = R_m + R_{p,i} + \left(R_{dc,i} + R_{sc,i}\right)$	(9)
Total resistance	$R_t = \sum_{i=1}^{N} R_{tS,i}$	(10)
Trans-membrane pressure	$TMP = \mu J R_t$	(11)

Notes: μ_s = sludge viscosity; d_p= particle diameter; J = permeate flux; C_d = lifting force coefficient; C_{ss} = suspended solid concentration of biomass sludge; γ = compression coefficient for dynamic sludge layer; V_f = volume of permeate produced; β = erosion rate coefficient of dynamic sludge film; α = stickiness of biomass; η_c = efficiency of backwashing; C_{sm} = concentration of COD at the physical membrane surface; C_s = concentration of COD in the mixed liquor at the physical membrane surface; $R_{tS,i}$ = total resistance of fouling in the section i; R_m = intrinsic resistance of the membrane; $R_{p,i}$ = the pore fouling resistance caused by solute deposition inside the membrane pores in the section i; $R_{C,i}$ = resistance of cake layer in the section i; $R_{dc,i}$ = resistance of dynamic sludge film in the section i; $R_{sc,i}$ = resistance of stable sludge cake in the section i; R_t = total fouling resistances.

concentration (C_S) modelled by means the biological sub-model (Eq. (8), Table 1). The physical sub-model is also able to reproduce for each horizontal cross membrane areal i the total resistance ($R_{tS,i}$) as the sum of the membrane resistance (R_m), the pore fouling resistance ($R_{p,i}$) and the resistance of cake layer ($R_{c,i}$) (Eq. (9), Table 1). This latter is considered as the sum of the dynamic sludge film ($R_{dc,i}$) and of stable sludge cake resistance attached onto the membrane surface ($R_{sc,i}$). The total resistance R_t is computed as the sum of $R_{tS,i}$ of all the N horizontal cross membrane areal sections (Eq. (10), Table 1). Finally, the trans-membrane variation is modelled according to Eq. (11) of Table 1.

The entire plant model was coded in Fortran.

The model has been applied to an UCT-MBR pilot plant (Fig. 1). The pilot plant consists of three reactors in series, anaerobic (section 1), anoxic (section 2) and aerobic (section 3), respectively, followed by an aerobic tank (section 4) where two hollow fibre membrane modules (Zenon Zeeweed, ZW 10) are submerged and a tank where permeate is stored (section 5) [10].

In order to maintain the required biomass concentration for biological activity, recycled fluxes are considered from membrane tank to aerobic tank, from aerobic to anoxic tank and from anoxic to anaerobic tank. The pilot plant has been operated for 165 days feeding with 40 L/h of municipal wastewater. During this period, samples of composite influent wastewater (section 0), grab mixed liquor in sections 1–4 and the permeate (section 5) were collected three times per week. Samples were analysed for total and volatile suspended solids (TSS and VSS), total and soluble COD, NH_4–N, NO_2–N, NO_3–N, N_{TOT}, P_{TOT} [27].

Further details about the pilot plant, field gathering campaign and the integrated mathematical model the reader is referred to literature [10,24].

2.2. The GSA-GLUE approach for the uncertainty assessment

In this study, the uncertainty assessment was carried out by using the GSA-GLUE approach formerly proposed by Ratto et al. [22]. Here, the GSA-GLUE approach is used to assess uncertainty with slight difference compared to the original approach proposed by Ratto et al. [22]. In particular, two main differences have been here introduced: (1) the likelihood measure (employed to quantify the goodness of the model predictions with respect to the observations); (2) the employed GSA method. The GSA-GLUE approach has the peculiarity to consider the likelihood, related to the variation of each factor, as a further model output for the GSA application. This means that factors, that are important for the likelihood surface and non-influential for the simulated model outputs, can be selected and included in the uncertainty analysis [23]. As reported in Fig. 2, the GSA-GLUE approach applied here consists of three main phases sub-divided in three main different steps: (A) preliminary choices; (B) GSA and (C) GLUE. In the following, each step is discussed in detail. The term "model factors or factors" includes model parameters and input variables of the model under study. The term "variable" indicates the model outputs and related likelihood

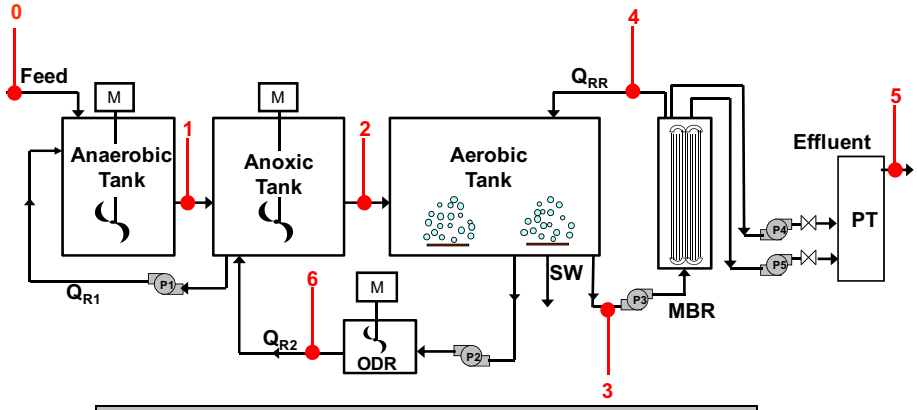

LEGEND			
M	Mixer	Q_{R1}-Q_{R2}	Mixed Liquor Recycle
PT	Permeate tank	RR	Retained Recycle
P1-P2- P3	Pump of the mixed liquor recycle	SW	Sludge wasting
P4- P5	Permeate extraction pump		Bidirectional valve
ODR	Oxygen Depletion Reactor		Sampling section point

Fig. 1. Schematic overview of the UCT-MBR pilot plant.

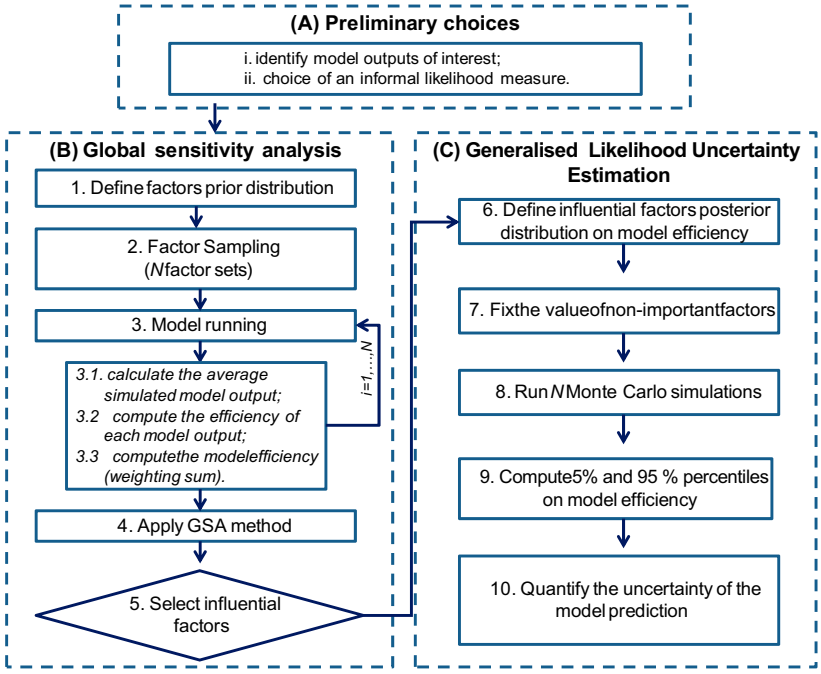

Fig. 2. Flow chart of the GSA-GLUE approach applied: (A) preliminary choices; (B) GSA application and (C) GLUE application.

measure, used as reference for the GSA-GLUE application.

2.2.1. Phase A: preliminary choices

The first phase of the GSA-GLUE approach consists of: (i) the identification of the model outputs to focus on and (ii) the selection of the informal likelihood measure to adopt. The selection of the model outputs depends on the main aim of the modeller, e.g. in case the modeller aims at the quantification of the model uncertainty related to the nitrogen removal processes, it is suggested to consider the ammonia and nitrate as reference model outputs.

As demonstrated in literature, the selection of the informal likelihood measure can have relevant implications on the results [23,28]. Thus, in this context, it is suggested to use the likelihood measure that, on the basis of the modeller's experience, is much more suitable for the model under study.

2.2.2. Phase B: GSA application

The GSA is able to provide information on how model outputs are influenced by the simultaneous variation of input factors [14]. When the modeller is mainly interested in the uncertainty assessment, GSA can help to better explain the model structure and the sources of uncertainty [22]. The second phase of the GSA-GLUE approach represents the GSA application. This phase is divided into five connected sequential steps (Fig. 2, steps 1–5). The GSA application begins with the definition of the prior distribution of the involved factors (step 1 of Fig. 2). In particular, a prior distribution and the variation range of each factor have to be defined. Due to the lack of a priori information on model factors, a uniform prior distribution is preferred. In step 2 of Fig. 2, the sampling of N model factor sets is performed. In this study, N factor sets have been generated by means of the Latin hypercube sampling method [29]. The N sampled factor sets are used for running Monte Carlo simulations (step 3 of Fig. 2). For each simulation, the time average of the selected model outputs (step 3.1 of Fig. 2), the efficiency of each model output (step 3.2 of Fig. 2) and the model efficiency (E_{MOD}) (step 3.3 of Fig. 2) are computed as discussed in the following paragraph. Thereafter, the GSA method is applied (step 4 of Fig. 2). After applying the GSA method, the important factors for the considered model outputs are selected (step 5 of Fig. 2).

2.2.3. Phase C: GLUE application

The GLUE method is based on Monte Carlo simulations [20]. Specifically, a large number of model

factor sets is randomly generated from a prior distribution. The model is run for each generated set. The acceptability of each set is assessed by comparing predicted to observed data throughout a chosen likelihood measure/efficiency. On the basis of a threshold value of the likelihood measure, the factor sets are divided in two categories: behavioural and no behavioural [20].

Specifically, the GLUE application is composed of six steps (from step 6 to step 10 of Fig. 2). The first step represents the definition of the posterior distribution for the important factors, selected by means of GSA application phase (step 6 of Fig. 2). Following the GSA application for the GLUE application, only the set of important factors is considered. Conversely, the unimportant factors are fixed at their calibrated value (step 7 of Fig. 2). For the important model factors, the posterior distribution, conditioned to the measured data, is then computed on the basis of the cumulated likelihood distribution of E_{MOD}. Thereafter, N Monte Carlo simulations are performed varying only the important factors simultaneously by using the posterior distribution (step 8 of Fig. 2). For each factors set, a likelihood measure of each variable is computed. Subsequently, the 5th and 95th percentiles of the model cumulative likelihood distributions are computed (step 9 of Fig. 2) and the uncertainty bands of each model output are drawn (step 10 of Fig. 2).

In the last step of the GLUE application (step 10 of Fig. 2), for each model output, the quantification of the uncertainty of the prediction bands (step 10 of Fig. 2) is performed. Regarding the uncertainty assessment, different indices can be used. In this study, the uncertainty is quantified considering six indices: the maximum band width (max_{WDTH}), the average band width ($average_{WDTH}$), the ratio $max_{WDTH}/average_{WDTH}$, the greatest distance between the calibrated simulation and the 5% (D_max 5%) and 95% (D_max 95%) uncertainty bands and the average relative interval length (ARIL).

For each model output, max_{WDTH} and $average_{WDTH}$ quantify, respectively, the maximum and the average degree of uncertainty related to that variable. Conversely, the ratio $max_{WDTH}/average_{WDTH}$ provides a measure of the stability of the uncertainty degree over the entire simulation period. A value close to 1 indicates that the same uncertainty is provided during the simulation. The ARIL of the j-th model output ($ARIL_{,j}$) is computed as follows [30]:

$$ARIL_j = \frac{1}{N_{meas}} \sum_{k=1}^{N_{meas}} \frac{Limit_{upper,k} - Limit_{lower,k}}{Y_j(t_k)} \quad (12)$$

where N_{meas} represents the number of measured data available for the j-th model output; $Limit_{upper,k}$ and $Limit_{lower,k}$ represent, respectively, the upper and the lower band value at the time t_k and $Y_j(t_k)$ is the measured value of the model output j related to the time t_k. Smaller is the $ARIL_{,j}$ value, better is the model performance for the j-th model output.

2.3. The GSA-GLUE application

In the following, details on the GSA-GLUE application for this study are provided. The GSA-GLUE was applied considering only the model parameters as factors and without exploring any variation of the other input variables. Specifically, as reference variables, we considered twelve simulated model outputs (j), twelve likelihood (E_j) corresponding to each jth model output and the overall model efficiency (E_{MOD}). This study is mainly focused on the effluent quality; the following model outputs have been taken into account: total COD ($COD_{TOT,1}$), ammonia ($S_{NH4,1}$), orthophosphate ($S_{PO,1}$), mixed liquor suspended solid ($MLSS_1$), $COD_{TOT,2}$, $S_{NH4,2}$, $S_{PO,2}$, (soluble COD) $COD_{SOL,3}$, $S_{NH4,3}$, $MLSS_3$, $S_{NH4,5}$ and nitrate ($S_{NO3,5}$), (the numbers in the subscript indicate the plant sections of reference). However, it is important to precise that since the model structure is integrated (both physical and biological phenomena are modelled), the overall analysed quality model outputs take into account the influence of membrane fouling. Concerning the likelihood of the j-th model output (E_j), similar to previous studies [10,31,32], the following expression was employed:

$$L(\theta_i/Y_j) = E_j = \exp\left(\frac{-\sigma^2_{Mj-Oj}}{\sigma^2_{Oj}}\right) \quad (13)$$

where θ_i represents the ith set of model factor (randomly generated), σ^2_{Mj-Oj} is the sum of squared errors between model output (M_j) and observation (O_j) of the j-th variable, and σ^2_{Oj} is the sum of squared errors between the observations and the average value of the observations for the period under consideration. Moreover, for each ith set of model factors, $E_{MOD,i}$ was computed as the weighted sum of the likelihood, $L(\theta_i/Y_j)$, of the twelve simulated model outputs taken into account (Eq. (14)).

For each model output j, the weight (α_j) has been computed by dividing the maximum value of the likelihood measure of the model output j by the sum of the maximum values of the likelihood measures of the other model outputs [31]:

$$E_{\mathrm{MOD,i}} = \sum_{j=1}^{12} \alpha_j L\left(\theta_i / Y_j\right) \quad (14)$$

Similar to previous studies, the variation range of each factor was defined by varying of +/–5% the calibration factor value assuming a uniform distribution, in order to analyse the model behaviour around the calibration values [19,33].

In this study, the sensitivity analysis has been performed by using the SRC method. The selection of the SRC method, in place of other GSA methods suggested in literature such as the variance-based methods, allows in case of linear models, substantial reduction of the computational cost [9,11]. For linear model, the SRC method is able to identify factors (model parameter and model input variables) which affect or not the model variance and allows also to satisfactorily decompose the model variance. All the 79 model factors reported in Table 2 have been considered during the GSA application. The SRC method consists of performing a multivariate linear regression between the model outputs (y) and inputs (x) by using Monte Carlo simulations (with random sampling of inputs). The standardised regression slope (β_i), computed according to Eq. (15), represents a valid measure of sensitivity [14].

$$\mathrm{SRC}(x_i) = \beta_i = b_i \cdot \sigma_{x_i} / \sigma_y \quad (15)$$

where σ_{xi} and σ_y represent the factor and model output standard deviation, respectively. The goodness of SRC as a measure of sensitivity is indicated by the coefficient of determination R^2, which represents the portion of total variance explained by the regression model; this value has to be greater than 0.7 (for linear model R^2 is close to 1) [14]. The sign of β_i indicates its positive (sign +) or negative (sign –) effect on the model output variation [19]. The SRC method generally requires a number of MCs in the range of 500—1,000 in the case of random sampling. Model factors were selected as important whenever the absolute value of β_i was greater than 0.2 at least for one of the variables (twelve model outputs, efficiency of each model output and E_{MOD}). In case of quite linear behaviour of the model ($R^2 > 0.7$), the threshold of 0.2 represents that the variation of the model factor causes the 4% variation of the model output (in terms of first-order effect). In this study, the number N of Monte Carlo simulations was selected according to previous studies. In particular, the uncertainty analysis was carried out by using a different number of simulations starting from 200 and increasing with steps of 200. At each step, the cumulated likelihood distributions were compared to those of the previous step. The number of Monte Carlo simulations for which the difference between the distributions was lower than 0.01, in terms of Kolmogorov—Smirnov maximum distance, was considered appropriate for the analysis. Regarding the GLUE application, the behavioural Monte Carlo simulations have been selected, employing a threshold value of zero.

3. Results and discussion

3.1. GSA application

In order to apply the SRC method, 800 Monte Carlo simulations have been performed for each model factor. The number of simulations was established on the basis of the procedure based on Kolmogorov—Smirnov test. Table 3 summarises the results of the SRC related to the model factors to which at least one of the variable is important. The linear model determination coefficients (R^2), obtained applying the SRC method, for the variables taken into account were always >0.7 except for $\mathrm{COD_{TOT,1}}$, $\mathrm{COD_{TOT,2}}$, $S_{\mathrm{NH4,5}}$, $E_{\mathrm{CODTOT,1}}$, $E_{\mathrm{CODTOT,2}}$ and $E_{\mathrm{SNH4,5}}$ (Table 3). The low R^2 values for $\mathrm{COD_{TOT,1}}$, $\mathrm{COD_{TOT,2}}$, $S_{\mathrm{NH4,5}}$, $E_{\mathrm{CODTOT,1}}$, $E_{\mathrm{CODTOT,2}}$ and $E_{\mathrm{SNH4,5}}$ are likely due to the interactions among the model factors involved. This is most likely related to the fact that the $\mathrm{COD_{TOT,1}}$ and $\mathrm{COD_{TOT,2}}$ are a combination of different model outputs. As the average value of R^2 is close to 0.7, the individual contribution of each model factor to the total variance of the model outputs taken into account has been calculated by means of β_i^2. Moreover, the value of R^2 here obtained demonstrates that the simulated model outputs can be adequately described as a linear function of the model factors and β_i can be used as a valuable measure of sensitivity.

Previous application of the SRC method to the same model has shown that the SRC method is outside of its range of applicability when the widest variation range found in literature is used for the model factors [34]. Here, a narrower variation range of model factors (+/–5% respect to the calibration value) has been explored; thus, a quite high value of R^2 has been obtained.

By applying the SRC, it has been obtained that 65% of model factors (51 on 79) can be fixed anywhere within their range of uncertainty without affecting uncertainty of the variables taken into account (Table 3). Conversely, 28 model factors were important at least for one of the variables taken into account, thus reducing to 28 the number of factors to be

Table 2
Description, symbol, unit, variation range, calibrated value, broadest literature variation range and reference for each model factor

Description	Symbol	Unit	MIN	MAX	Calibrated	Literature range	References
Maximum specific hydrolysis rate	k_H	g X_Sg X_H^{-1} d^{-1}	1.639	1.811	1.72	1.05–4.5	[33]
Correction factor for hydrolysis under anoxic conditions	$\eta_{NO3,HYD}$	—	0.570	0.630	0.60	0.402–0.798	[35]
Correction factor for hydrolysis under anaerobic conditions	η_{FE}	—	0.455	0.502	0.48	0.2–0.6	[35]
Half saturation parameter for SO_2 for X_H	K_O	g S_{O2} m^{-3}	0.512	0.566	0.54	0.1–1	[36]
Half saturation parameter for S_{NO3} for X_H	K_{NO3}	g S_{NO3} m^{-3}	0.300	0.331	0.32	0.1–0.625	[33,36]
Half saturation parameter for X_S/X_H	K_X	g X_S g X_H^{-1}	0.095	0.105	0.10	0.05–0.15	[33]
Half saturation/inhibition parameter for SO_2	$K_{O,HYD}$	g S_{O2} m^{-3}	0.190	0.210	0.20	0.1–0.3	[33]
Half saturation/inhibition parameter for S_{NO3}	$K_{NO3,HYD}$	g N m^{-3}	0.475	0.525	0.50	0.375–0.625	[33]
Maximum growth rate of X_H	μ_H	d^{-1}	1.235	1.365	1.30	0.6–13.2	[4]
Rate constant for fermentation/Maximum specific fermentation growth rate	q_{FE}	g S_F g X_H^{-1} d^{-1}	2.850	3.150	3.00	1.5–4.5	[33]
Reduction factor for anoxic growth of X_H	$\eta_{NO3,H}$	–	0.936	1.034	0.99	0.6–1	[33]
Decay rate for X_H	b_H	d^{-1}	0.554	0.612	0.58	0.05–1.6	[4]
Half saturation parameter for S_F	K_F	g S_F m^{-3}	3.800	4.200	4.00	2–6	[33]
Half saturation parameter for fermentation of S_F	K_{FE}	g S_F m^{-3}	3.800	4.200	4.00	2–6	[33]
Half saturation parameter for S_A	K_A	g S_A m^{-3}	3.800	4.200	4.00	2–6	[33]
Half saturation parameter for S_{NH4} for X_H	$K_{NH,H}$	g S_{NH4} m^{-3}	0.091	0.100	0.10	0.02–2	[35]
Half saturation parameter for S_{PO4} for X_H	K_P	g S_{PO4} m^{-3}	0.010	0.011	0.01	0.005–0.015	[33]
Half saturation parameter for S_{ALK} for X_H	$K_{ALK,H}$	mol HCO_3^- m^{-3}	0.095	0.105	0.10	0.05–0.15	[33]
Rate constant for S_A uptake rate	q_{PHA}	g X_{PHA} g X_{PAO}^{-1} d^{-1}	3.514	3.884	3.70	0.3–5.7	[35]
Rate constant for storage of polyphosphates	q_{PP}	g X_{PP} g X_{PAO}^{-1} d^{-1}	2.224	2.458	2.34	0–3.3	[35]
Maximum growth rate of X_{PAO}	μ_{PAO}	d^{-1}	0.681	0.753	0.72	0.5–1.5	[33]
Reduction factor for anoxic growth of X_{PAO}	$\eta_{NO3,PAO}$	—	0.570	0.630	0.60	0.45–0.75	[33]
Endogenous respiration rate of X_{PAO}	b_{PAO}	d^{-1}	0.223	0.247	0.24	0.1–0.25	[35]

(*Continued*)

Table 2 (*Continued*)

Description	Symbol	Unit	MIN	MAX	Calibrated	Literature range	References
Rate constant for Lysis of polyphospates	b_{PP}	d^{-1}	0.190	0.210	0.20	0.1–0.25	[35]
Rate constant for respiration of X_{PHA}	b_{PHA}	d^{-1}	0.190	0.210	0.20	0.1–0.25	[35]
Half saturation parameter for S_{PO4} uptake	K_{PS}	g S_{PO4} m^{-3}	0.190	0.210	0.20	0.1–0.3	[33]
Maximum ratio of X_{PP}/X_{PAO}	K_{PP}	g X_{PP} g X_{PAO}^{-1}	0.010	0.011	0.01	0.005–0.015	[33]
Half saturation parameter for X_{PP}/X_{PAO}	K_{MAX}	g X_{PP} g X_{PAO}^{-1}	0.323	0.357	0.34	0.2–0.51	[4]
Half inhibition parameter for X_{PP}/X_{PAO}	K_{IPP}	g X_{PP} g X_{PAO}^{-1}	0.019	0.021	0.02	0.01–0.03	[33]
Saturation constant for X_{PHA}/X_{PAO}	K_{PHA}	g X_{PHA} g X_{PAO}^{-1}	0.010	0.011	0.01	0.005–0.015	[33]
Half saturation parameter for SO_2 for X_{PAO}	$K_{O,PAO}$	g S_{O2} m^{-3}	0.190	0.210	0.20	0.1–0.3	[33]
Half saturation parameter for S_{NO3} for X_{PAO}	$K_{NO3,PAO}$	g S_{NO3}.m^{-3}	0.475	0.525	0.50	0.375–0.625	[33]
Half saturation parameter for S_A for X_{PAO}	$K_{A,PAO}$	g S_A m^{-3}	3.800	4.200	4.00	2–6	[33]
Half saturation parameter for S_{NH4} for X_{PAO}	$K_{NH,PAO}$	g S_{NH4} m^{-3}	0.048	0.053	0.05	0.025–0.075	[33]
Half saturation parameter for S_{PO4} as nutrient (X_{PAO} growth)	$K_{P,PAO}$	g S_{PO4} m^{-3}	0.010	0.011	0.01	0.005–0.015	[33]
Half saturation parameter for S_{ALK} for X_{PAO}	$K_{ALK,PAO}$	mol HCO_3^- m^{-3}	0.095	0.105	0.10	0.05–0.15	[33]
Maximum growth rate of X_{AUT}	μ_{AUT}	d^{-1}	1.122	1.240	1.18	0.2–1.2	[35]
Decay rate for X_{AUT}	b_{AUT}	d^{-1}	0.076	0.084	0.08	0.04–0.1605	[35]
Half saturation parameter for SO_2 for X_{AUT}	$K_{O,A}$	g S_{O2}.m^{-3}	0.475	0.525	0.50	0.1–2	[4,36]
Half saturation parameter for S_{NH4} for X_{AUT}	$K_{NH,A}$	g S_{NH4} m^{-3}	0.950	1.050	1.00	0.5–1.5	[35]
Half saturation parameter for S_{ALK} for X_{AUT}	$K_{ALK,A}$	mol HCO_3^- m^{-3}	0.475	0.525	0.50	0.25–0.75	[33]
Half saturation parameter for S_{PO4} for X_{PAO}	$K_{P,A}$	g S_{PO4} m^{-3}	0.010	0.011	0.01	0.005–0.015	[33]
Hydrolysis rate coefficient for S_{BAP}	$k_{H,BAP}$	d^{-1}	7.04E-07	7.78E-07	7.41E-07	3.705E-07–1.11E-06	[24]
Hydrolysis rate coefficient for S_{UAP}	$k_{H,UAP}$	d^{-1}	0.010	0.011	0.01	0.0051–0.0153	[24]
Overall oxygen transfer coefficient aerobic tank	$k_{LaT,3}$	h^{-1}	9.500	10.500	10.00	9.5–10.5	[4]
Overall oxygen transfer coefficient MBR tank	$k_{LaT,4}$	h^{-1}	3.230	3.570	3.40	3.23–3.57	[4]
Yield for X_H growth	Y_H	g X_H g X_S^{-1}	0.372	0.411	0.39	0.38–0.75	[4]
Fraction of X_I generated in biomass decay	f_{XI}	g X_I g X_H^{-1}	0.057	0.063	0.06	0.05–0.4	[36]
Yield for X_{PAO} growth	Y_{PAO}	g X_{PAO} g X_{PHA}^{-1}	0.421	0.465	0.44	0.42–0.78125	[33]
Yield for X_{PP} requirement per X_{PHA} stored	Y_{PO4}		0.380	0.420	0.40	0.38–0.42	[33]

(*Continued*)

Table 2 (*Continued*)

Description	Symbol	Unit	MIN	MAX	Calibrated	Literature range	References
Yield for X_{PP} storage per X_{PHA} utilised	Y_{PHA}	g X_{PP} g X_{PHA}^{-1}	0.190	0.210	0.20	0.19–0.21	[33]
Yield of X_{AUT} growth per S_{NO3}	Y_A	g X_{AUT} g S_{NO3}^{-1}	0.228	0.252	0.24	0.228–0.252	[33]
Fraction of S_{BAP} generated in biomass decay	f_{BAP}	—	0.007	0.007	0.0070	0.0069–0.022575	[33]
Fraction of S_{UAP} generated in biomass decay	f_{UAP}	—	0.091	0.101	0.10	0.091485–0.101115	[33]
Fraction of influent S_F	F_{SF}	—	0.114	0.126	0.12	0.06–0.18	[33]
Fraction of influent S_A	F_{SA}	—	0.040	0.045	0.04	0.04–0.12	[33]
Fraction of influent S_I	F_{SI}	—	0.114	0.126	0.12	0.114–0.126	[33]
Fraction of influent X_I	F_{XI}	—	0.095	0.105	0.10	0.05–0.15	[33]
Fraction of influent X_H	F_{XH}	—	0.095	0.105	0.10	0.06–0.18	[33]
Erosion rate coefficient of the dynamic sludge	β	—	0.013	0.014	0.01	0.0001–0.021	[31]
Stickiness of the biomass particles	α	—	0.454	0.502	0.48	0–1	[31]
Compressibility of cake	γ	kg m^{-3} s	0.0023	0.0025	0.0024	0.000556–0.00278	[31]
Substrate fraction below the critical molecular weight	f	—	0.865	0.956	0.91	0.001–0.99	[31]
Screening parameter	λ	m^{-1}	1.44E+03	1.60E+03	1.52E+03	1 E+03–2E+03	[31]
Efficiency of backwashing	C_E	—	0.946	1.046	0.9960	0.996−0.999	[31]
N content of S_I	$i_{N,SI}$	g N g S_I^{-1}	0.010	0.011	0.01	0.0075–0.0125	[33]
N content of S_F	$i_{N,SF}$	g N g S_F^{-1}	0.029	0.032	0.03	0.0225–0.0375	[33]
N content of X_I	$i_{N,XI}$	g N g X_I^{-1}	0.023	0.026	0.0245	0.015–0.025	[33]
N content of X_S	$i_{N,XS}$	g N g X_S^{-1}	0.041	0.046	0.0437	0.03–0.05	[33]
N content of biomass	$i_{N,BM}$	g N g X_{BM}^{-1}	0.010	0.011	0.01	0.0665–0.0735	[33]
P content of S_F	$i_{P,SF}$	g P g S_F^{-1}	0.029	0.032	0.03	0.005–0.015	[33]
P content of X_I	$i_{P,XI}$	g P g X_I^{-1}	0.005	0.006	0.0056	0.005–0.015	[33]
P content of X_S	$i_{P,XS}$	g P g X_S^{-1}	0.009	0.010	0.0099	0.005–0.015	[33]
N content of biomass	$i_{P,BM}$	g P g X_{BM}^{-1}	0.020	0.022	0.0207	0.015–0.025	[33]
Conversion factor X_I in TSS	$i_{TSS,XI}$	g TSS g X_I^{-1}	0.748	0.827	0.79	0.7125–0.7875	[33]
Conversion factor X_S in TSS	$i_{TSS,XS}$	g TSS g X_S^{-1}	0.748	0.827	0.79	0.7125–0.7875	[33]
Conversion factor biomass in TSS	$i_{TSS,BM}$	g TSS g X_{BM}^{-1}	0.898	0.992	0.95	0.855–0.945	[33]
Conversion factor X_{PHA} in TSS	$i_{TSS,XPHA}$	g TSS g X_{PHA}^{-1}	0.570	0.630	0.60	0.57–0.63	[33]
Conversion factor X_{PP} in TSS	$i_{TSS,XPP}$	g TSS g X_{PP}^{-1}	3.069	3.392	3.23	3.0685–3.3915	[33]

considered for the GLUE application. The results of GSA application provides useful hints for identifying which factors, once evaluated, may provide a reduction of the model variance and consequently which model outputs need further experimental measures.

In the following, for sake of conciseness, only the results related to six model variables ($MLSS_1$, $S_{PO,1}$, $E_{SPO,1}$, $S_{NH4,3}$, $S_{NO3,5}$ and E_{MOD}) will be discussed, focusing the attention on the physical/biological meaning of the important factors obtained for each variable. These variables have been selected, among the available measured ones, as representative of the main processes occurring in each reactor. For instance, in the anaerobic tank, the most important process is

Table 3
Results of the SRC application (β_i, R^2) for each model output only for the factors resulted to be important at least for one output

	Model outputs												Efficiencies											
	$COD_{TOT,1}$	$S_{NH4,1}$	$S_{PO,1}$	$MLSS_1$	$COD_{TOT,2}$	$S_{NH4,2}$	$S_{PO,2}$	$COD_{SOL,3}$	$S_{NH4,3}$	$MLSS_3$	$S_{NH4,5}$	$S_{NO3,5}$	E_{MOD}	$E_{CODTOT,1}$	$E_{SNH4,1}$	$E_{SPO,1}$	$E_{MLSS,1}$	$E_{CODTOT,2}$	$E_{SNH4,2}$	$E_{SPO,2}$	$E_{CODSOL,3}$	$E_{SNH4,3}$	$E_{MLSS,3}$	$E_{SNH4,5}$	$E_{SNO3,5}$
R^2	0.51	0.82	0.72	0.74	0.3	0.71	0.68	0.68	0.72	0.75	0.51	0.82	0.72	0.47	0.78	0.65	0.71	0.27	0.69	0.68	0.64	0.71	0.70	0.50	0.75
Symbol	β_i												β_i												
K_O	0.05	0.07	0.11	0.04	0.05	0.06	0.11	−0.02	−0.11	0.04	0.01	0.00	0.10	0.03	0.07	0.21	0.04	0.05	0.06	0.21	0.02	0.22	0.04	0.01	−0.01
μ_H	−0.35	0.02	0.00	−0.02	0.01	0.00	0.00	0.14	−0.05	−0.02	−0.05	−0.35	0.04	0.33	0.03	0.00	0.00	0.02	0.03	0.00	0.17	0.02	−0.01	0.02	0.27
$\eta_{NO3,H}$	−0.01	−0.05	−0.04	0.01	−0.01	−0.04	−0.04	0.02	0.04	0.01	−0.14	−0.17	−0.04	0.01	−0.07	−0.05	0.01	−0.01	−0.03	−0.04	−0.02	−0.01	0.01	−0.22	−0.12
K_P	0.02	0.07	0.16	0.05	0.02	0.08	0.21	−0.12	0.10	0.05	0.09	0.00	−0.05	−0.01	0.06	0.05	0.05	0.02	0.08	0.25	0.11	−0.23	0.05	−0.12	0.00
μ_{AUT}	−0.03	−0.11	−0.03	−0.01	−0.04	−0.48	−0.03	0.08	−0.33	−0.01	0.24	0.05	−0.04	−0.02	−0.12	−0.03	−0.02	−0.04	−0.43	−0.03	−0.04	0.12	−0.02	−0.11	−0.05
b_{AUT}	−0.03	0.01	−0.03	−0.03	−0.03	0.32	−0.04	−0.04	0.23	−0.03	−0.23	0.00	−0.08	−0.02	0.02	−0.03	−0.02	−0.03	0.32	−0.03	0.04	−0.19	−0.02	−0.19	−0.01
$K_{O,A}$	−0.05	0.01	−0.04	−0.01	−0.04	0.03	−0.04	−0.03	0.10	−0.01	0.30	0.07	−0.09	−0.05	−0.01	−0.04	0.00	−0.05	0.03	−0.04	0.00	−0.07	0.00	−0.17	−0.08
$K_{NH,A}$	0.05	0.00	−0.11	0.07	0.06	0.11	−0.12	−0.07	−0.22	0.07	−0.02	−0.03	−0.02	0.04	0.00	−0.21	0.08	0.06	−0.11	−0.11	0.06	0.14	0.08	0.04	0.02
$K_{P,A}$	0.05	0.11	0.01	−0.02	0.00	0.10	0.01	0.08	0.03	−0.02	0.03	−0.06	0.01	0.01	0.30	0.01	−0.02	−0.01	0.10	0.01	−0.07	0.01	−0.02	0.02	0.05
Y_H	−0.05	0.03	0.00	0.33	−0.04	0.12	0.00	−0.03	−0.01	0.23	0.32	−0.35	0.01	−0.04	0.03	0.00	−0.33	−0.04	0.12	0.00	−0.02	0.02	−0.23	0.03	0.34
f_{XI}	0.01	0.06	0.02	−0.22	0.02	0.05	0.01	−0.05	0.02	0.12	0.02	0.00	0.00	0.02	0.06	0.02	−0.21	0.03	0.05	0.02	0.05	−0.05	−0.21	−0.03	−0.01
Y_{PAO}	0.05	0.00	0.16	0.01	0.04	0.00	−0.06	0.04	−0.05	0.01	−0.04	0.00	0.06	0.05	0.00	−0.06	0.01	0.04	0.00	−0.06	0.00	0.23	0.01	0.11	0.00
f_{BAP}	−0.04	0.20	0.12	−0.01	0.14	0.09	−0.02	−0.19	0.04	−0.01	0.04	−0.08	−0.03	−0.04	0.39	−0.02	−0.02	−0.05	0.09	−0.02	−0.01	−0.03	−0.02	−0.01	0.07
F_{SA}	0.13	0.02	0.01	0.03	0.03	0.01	0.01	−0.01	−0.06	0.03	−0.06	−0.02	0.02	0.25	0.03	0.01	0.02	0.02	0.01	0.00	0.02	0.00	0.02	0.01	0.04
F_{XI}	−0.02	0.03	−0.02	0.40	0.11	0.04	−0.02	−0.06	0.06	0.43	0.07	0.06	0.02	−0.05	0.01	−0.02	0.23	−0.02	0.05	−0.02	0.07	0.02	0.32	0.02	−0.08
γ	0.01	0.32	0.04	−0.13	−0.22	−0.22	−0.24	−0.06	0.01	0.03	0.01	−0.56	−0.76	0.04	0.52	0.04	0.14	0.12	0.01	0.24	0.06	0.00	0.04	0.01	0.36
f	−0.43	0.05	−0.01	−0.01	−0.02	0.05	−0.01	0.01	0.00	−0.31	0.01	−0.06	0.03	−0.23	0.04	−0.01	−0.02	−0.03	0.25	−0.01	−0.03	0.05	−0.22	0.06	0.03
C_E	0.02	−0.08	0.03	0.14	0.00	−0.02	0.03	0.62	−0.11	0.04	−0.11	0.25	0.08	0.02	0.02	0.03	0.24	0.01	−0.02	0.03	−0.64	0.20	0.04	0.12	0.22
$i_{N,SI}$	0.02	0.14	−0.02	0.01	0.01	0.24	−0.02	0.04	−0.04	0.01	−0.04	0.05	−0.03	−0.03	−0.03	−0.02	0.01	0.01	−0.24	−0.02	−0.08	0.01	0.01	0.01	−0.04
$i_{N,SF}$	0.06	−0.18	0.07	0.11	0.07	−0.01	0.07	0.00	−0.01	0.11	−0.01	−0.03	0.09	0.05	−0.01	0.07	0.23	0.07	−0.01	0.07	0.05	0.01	0.11	0.02	0.03
$i_{N,XS}$	−0.02	0.12	−0.06	0.02	0.02	−0.04	−0.06	0.01	0.16	0.02	−0.07	0.12	−0.08	−0.04	−0.11	−0.06	0.01	−0.02	−0.03	−0.06	0.01	−0.25	0.02	−0.05	−0.12
$i_{N,BM}$	−0.02	0.17	0.06	0.02	−0.01	0.06	0.05	−0.03	0.43	0.02	0.13	−0.13	0.05	−0.02	0.16	0.06	0.02	−0.02	0.06	0.06	0.02	0.31	0.02	0.11	−0.12
$i_{P,SF}$	0.06	−0.02	0.22	0.00	0.17	−0.03	0.32	−0.04	−0.29	0.01	−0.02	0.00	−0.02	0.01	−0.01	−0.32	0.00	0.28	−0.03	−0.22	0.02	−0.22	0.00	−0.02	0.00
$i_{P,XI}$	0.06	0.01	−0.41	0.04	0.16	0.01	−0.30	0.01	0.12	0.04	0.01	−0.08	−0.05	0.06	0.01	−0.39	0.04	0.15	0.01	−0.29	0.03	−0.12	0.04	−0.02	0.07
$i_{P,XS}$	0.04	0.08	0.35	0.01	0.13	0.08	0.47	0.02	0.06	0.01	0.06	−0.01	0.13	0.05	0.06	0.28	0.01	0.13	0.08	0.17	−0.07	−0.01	0.01	−0.01	0.01
$i_{P,BM}$	−0.09	−0.02	0.30	−0.13	−0.19	0.00	0.16	−0.01	0.09	−0.13	0.09	0.05	−0.07	−0.09	−0.04	0.25	−0.33	−0.12	−0.03	0.25	−0.02	−0.09	−0.13	−0.10	−0.06
$i_{TSS,XI}$	0.02	−0.01	0.04	0.39	0.02	−0.01	0.04	−0.01	−0.03	0.49	−0.03	−0.01	0.05	0.01	−0.01	0.04	0.29	0.02	−0.01	0.14	0.04	0.01	0.29	0.01	0.01
$i_{TSS,BM}$	0.06	−0.02	−0.03	0.25	0.06	−0.03	−0.03	−0.02	−0.07	0.15	−0.07	−0.01	0.00	0.05	0.00	−0.03	0.15	0.05	−0.03	−0.03	0.02	0.01	0.05	0.01	0.03

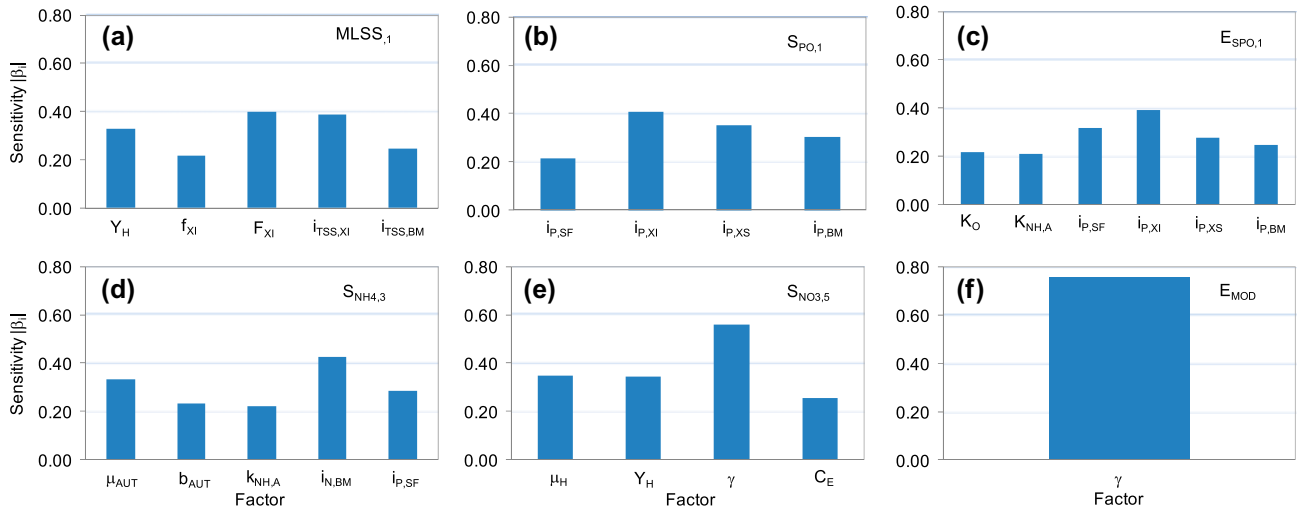

Fig. 3. Important model factors for $MLSS_1$ (a), $S_{PO,1}$ (b), $E_{SPO,1}$ (c), $S_{NH4,3}$ (d), $S_{NO3,5}$ (e) and E_{MOD} (f).

the release of phosphorus by the phosphorus-accumulating organisms (PAO). Therefore, S_{PO} is expected to vary the most in the anaerobic reactor. In Fig. 3, the $|\beta_i|$ values of the important model factors are shown for the six selected model outputs.

3.1.1. MLSS model outputs

For $MLSS_1$ only five model factors are important (Fig. 3(a), Table 3). Among them $i_{TSS,XI}$ and F_{XI} have the highest influence. These factors represent, respectively, the factor for converting the inert biomass (X_I) concentration into total suspended solid and the fraction of inert biomass in the inlet wastewater. Both $i_{TSS,XI}$ and F_{XI} are responsible for 15 and 16% of the total variance of $MLSS_1$, respectively. Thus, the experimental determination of F_{XI} by using batch respirometric tests for the influent COD fractionation leads to the 16% variance reduction for $MLSS_1$. The positive value of β_i for $i_{TSS,XI}$ and F_{XI} indicates that increasing the value of these two factors an increase of the $MLSS_1$ occurs. Moreover for $MLSS_1$ model factors Y_H (yield coefficient for X_H growth), f_{Xi} (fraction of X_i generated in biomass decay) and $i_{TSS,BM}$ (biomass conversion factor in total suspended solids) are important (Fig. 3(a), Table 3). As demonstrated in other studies, the influence of f_{Xi} is particularly interesting in MBR systems [9,34] with the increase of the sludge retention time (SRT). Indeed, the increase of SRT leads to the progressive accumulation of X_i. Consequently, in case of high SRT value (typical condition in MBRs) an important source of uncertainty determining the variance in the MLSS concentration is related to the biomass lysis process. Thus, it is important to know the activity of biomass by using respirometric method.

3.1.2. Phosphorus model outputs—P

For $S_{PO,1}$ factors $i_{P,SF}$, $i_{P,XI}$, $i_{P,XS}$ and $i_{P,BM}$ are important (Fig. 3(b)), which, respectively, represent the phosphorus content of soluble fermentable organic matter (S_F), X_I, particulate biodegradable organics (X_S) and biomass. Except for $i_{P,XI}$, all the important factors have positive influence on $S_{PO,1}$. The negative effect of $i_{P,XI}$ on $S_{PO,1}$ (increasing $i_{P,XI}$ the decrease of $S_{PO,1}$ occurs) is attributable to the fact that increasing the phosphorus content of X_I the S_{PO} produced during the anaerobic hydrolysis process is low. Such a result underlines, even for $S_{PO,1}$, that the proper knowing of the COD fractionation may lead to uncertainty reduction. The factors $i_{P,SF}$, $i_{P,XI}$, $i_{P,XS}$ and $i_{P,BM}$ are all related to phosphorus fractionation and no kinetic factors were important. From Table 3 and Fig. 3(c), one may observe that in terms of efficiency of the model output $S_{PO,1}$ the factors K_O and $K_{NH,A}$ as well as $i_{P,SF}$, $i_{P,XI}$, $i_{P,XS}$ and $i_{P,BM}$ are important. The importance of K_O on $S_{PO,1}$ is related to the ability of K_O to regulate the anoxic growth of heterotrophic biomass rate and consequently, the substrate availability. Such substrate availability is required for the anaerobic phosphorus release, recycled from the anoxic to the anaerobic tank. On the other hand, $K_{NH,A}$ regulates the rate of the aerobic growth of the autotrophic biomass and consequently the nitrate mass that arrives at the anaerobic

tank and which controls the anaerobic activity of PAOs. Thus, as the aerobic processes are quite important for the $S_{PO,1}$ modelling it is suggested, for systems having UCT scheme, to measure with specific test batch the value of $K_{NH,A}$ and K_O.

3.1.3. Nitrogen model outputs—N

Regarding $S_{NH4,3}$ factors μ_{AUT}, b_{AUT}, $K_{NH,A}$, $i_{N,BM}$ and $i_{P,SF}$ are important (Fig. 3(d)). The highest variance contribution is due to the factor $i_{N,BM}$ that is responsible for 18% of the $S_{NH4,3}$ total variance ($\beta_i^2 = 0.183$). Such a result demonstrates that even for the nitrogen variable, a high influence of the fractionation stochiometric coefficients is obtained. The influence of μ_{AUT} on $S_{NH4,3}$ is consistent with the nitrification process that occurs in the aerobic tank. Increasing μ_{AUT}, the aerobic growth rate of autotrophic biomass increases and, consequently, the ammonia concentration inside the aerobic tank decreases. This result has also been confirmed by the negative value of β_i of μ_{AUT} for $S_{NH4,3}$ ($\beta_i = -0.33$) which is in line with previous studies [34]. Thus, in order to reduce the uncertainty related to the nitrification process predictions, it is suggested to improve the knowledge acquired on the factors μ_{AUT} and b_{AUT}. Indeed, these two latter factors due to the typical different operating conditions of MBRs may have different values compared to the conventional systems. The influence of $i_{P,SF}$ is probably due to the indirect effect of this factor on the availability of nutrients for the biomass growth.

For $S_{NO3,5}$ factors μ_H, Y_H, γ and C_E are important (Fig. 3(e)). The influence of μ_H and Y_H is mainly related to the anoxic growth of heterotrophic organisms (denitrification process) occurring inside the anoxic tank that strongly influence the S_{NO3} concentration in the effluent. Indeed, denitrification occurs by means of heterotrophic biomass, thus increasing μ_H and Y_H, the effluent nitrate concentration decreases (as confirmed by the negative value of β_i related to μ_H and Y_H for $S_{NO3,5}$).

Factors γ and C_E (both related to the physical submodel) resulted also to be important. These model factors γ and C_E represent the compressibility of cake layer on the membrane surface and the efficiency of backwashing for membrane cleaning, respectively. Therefore, the results indicate that the presence of the membrane has a relevant contribution even for soluble pollutants removal such as S_{NO}. As demonstrated by the negative value of β_i related to γ for $S_{NO3,5}$, increasing the value of γ, a decrease of $S_{NO3,5}$ occurs. On the other hand, the positive value of β_i for C_E shows that increasing C_E, the increase of $S_{NO3,5}$ takes place. The influence of C_E and γ on $S_{NO3,5}$ can be due to the different ability, changing their value, of the cake layer to retain fraction of pollutants or to be interested of anoxic micro-zone. As shown in Fig. 3(f), the unique important factor for E_{MOD} is γ that contributes with almost 60% ($\beta_i^2 = 0.57$) to the total variance of E_{MOD}. Such a result has relevant interest for MBRs corroborating the fact, as demonstrated in previous studies [4,32,37], that the cake layer plays an important role on the pollutant removal.

3.2. GLUE application

Before applying the GLUE method, the posterior distributions of the important factors have been evaluated (step 6 of Fig. 2). The posterior distributions of the important factors have been obtained on the basis of the model efficiency. Thus, the obtained posterior distributions have been conditioned to the measured data allowing the model learning from the data. More specifically, for each important factor, the 800 model efficiencies (obtained as result of the step 3.3 of Fig. 2) have been ranked firstly on the basis of the increasing order of the important factor values. The ranked model efficiencies have been normalised with respect to the sum of the model efficiency values. For each important factor, the cumulative distribution of the normalised model efficiencies has been used for setting the posterior distribution. The GLUE was applied by performing 1,200 behavioural Monte Carlo simulations. During each simulation, only the 28 important model factors were varied (according to the range reported in Table 2 and the calculated posterior distribution). All non-important factors were kept constant and equal to their calibrated value.

In Table 4, the results of the indices used to quantify the uncertainty of the prediction bands are reported for each model output taken into account in the GSA-GLUE application.

In Fig. 4, the uncertainty bands of some model outputs are reported. In particular, the uncertainty bands for the following model outputs are shown: $COD_{TOT,1}$ (Fig. 4(a)), $S_{NH4,1}$ (Fig. 4(b)), $S_{PO,1}$ (Fig. 4(c)), $S_{PO,2}$ (Fig. 4(d)), $S_{NH4,3}$ (Fig. 4(e)) and $S_{NO3,5}$ (Fig. 4(f)).

From a visual inspection of Fig. 4, one may observe that the width of the uncertainty bands changes considerably with the model output. This result is corroborated by the statistical index values in Table 4. This is mainly due to the fact that some of the model outputs are involved in more complex phenomena than others (e.g. phosphorus or nitrogen removal processes). The different process complexity leads to high model prediction uncertainty [38]. Furthermore,

Table 4
Values of the indices computed for quantify the uncertainty of the prediction bands for each

	Model output										
PLANT SECTION	Anaerobic				Anoxic			Aaerobic			Effluent	
INDEX	$COD_{TOT,1}$	$S_{NH4,1}$	$S_{PO,1}$	$MLSS_1$	$COD_{TOT,2}$	$S_{NH4,2}$	$S_{PO,2}$	$COD_{SOL,3}$	$S_{NH4,3}$	$MLSS_3$	$S_{NH4,5}$	$S_{NO3,5}$
ARIL [–]	0.41	0.21	0.41	0.55	0.27	0.23	0.64	1.11	2.30	0.41	6.63	0.88
max_{WDTH} [mg/L]	1,449.43	2.22	4.83	1,702.15	1,291.87	2.19	8.23	116.40	1.62	2,404.29	1.70	12.81
$average_{WDTH}$ [mg/L]	1,369.91	1.84	4.03	1,627.79	1,231.85	1.80	7.18	63.21	0.49	2,298.69	0.58	10.88
$max_{WDTH}/average_{WDTH}$ [–]	1.06	1.21	1.20	1.05	1.05	1.21	1.15	1.84	3.31	1.05	2.95	1.18
D_max 5% [mg/L]	824.24	1.67	5.86	1,171.02	533.87	1.79	6.94	51.20	0.31	1,787.45	0.67	13.77
D_max 95% [mg/L]	1,132.38	1.89	6.77	1,055.48	930.88	1.71	9.06	81.57	1.36	1,037.02	1.13	19.04

Notes: ARIL = average relative interval length; max_{WDTH} = maximum band width; $average_{WDTH}$ = average band width; $max_{WDTH}/average_{WDTH}$ = ratio between max_{WDTH} and $average_{WDTH}$; D_max 5% = greatest distance between the calibrated simulation and the 5% percentile band; D_max 95% = greatest distance between the calibrated simulation and the 95% percentile band.

the overparameterisation (typical feature of the ASM models) and correlation among factors increase the factors uncertainty due to the low identifiability against the poor data availability. As shown in Table 4, high uncertainty, in terms of ARIL value, was obtained for the model outputs related to the nitrogen removal process ($S_{NH4,3}$; $S_{NH4,5}$; $S_{NO3,5}$). The high ARIL value shows that the model does not sufficiently reproduce the measured data. For $S_{NO3,5}$ this result could be due to the correlation between μ_{AUT} and b_{AUT} factors, both included in the GLUE application. Moreover, it is possible to observe that the uncertainty bands change with the plant section (Fig. 4). Such a result, as demonstrated also in previous studies on the ASM models, is mainly due to the different processes involved in the plant sections [34].

In the following, the results reported in Fig. 4 and in Table 4 are discussed in detail.

Regarding $COD_{TOT,1}$, the results show that the 62% of measured data lay inside the bands. Moreover, the low ARIL value (0.41) indicates that the model is sufficiently able to reproduce the measured data (Table 4, Fig. 4(a)). The $max_{WDTH}/average_{WDTH}$ (1.06) value for $COD_{TOT,1}$, being very close to 1, shows that over the entire simulation period, the model prediction uncertainty is constant.

The band width for the ammonia model outputs ($S_{NH4,1}$ and $S_{NH4,3}$) increases from the first to the third section (Fig. 4(b) and (e)) as demonstrated by the increasing value of ARIL throughout the plant sections (from 0.21 to 2.30 for sections 1 and 3, respectively) (see, Table 4). The larger uncertainty bands in section 3 are mainly due to two effects. The first effect is the nitrification process in the aerobic tank (section 3) which strongly influences the S_{NH4} concentration, unlike the biological processes that take place inside the anaerobic (section 1) or anoxic (section 2) tanks that do not affect the S_{NH4} concentration. Thus, the uncertainty of the model factors related to the nitrification process (μ_{AUT}, b_{AUT}, $K_{O,A}$) is mainly transferred to $S_{NH4,3}$. The second effect is the uncertainty propagation from the influent to the effluent, which makes the uncertainty of the last plant sections higher than others. Moreover, the value of $max_{WDTH}/average_{WDTH}$ obtained for $S_{NH4,1}$ and $S_{NH4,3}$ corroborates the results related to the ARIL values discussed above. The low value of $max_{WDTH}/average_{WDTH}$ for $S_{NH4,1}$ (1.21,) shows that the model prediction uncertainty for $S_{NH4,1}$ is almost constant and no temporal variation of the band's width along the simulation period occurs. Such a result suggests that the uncertainty of the input factors has a low influence on the uncertainty of $S_{NH4,1}$ prediction. This result is related to the fact

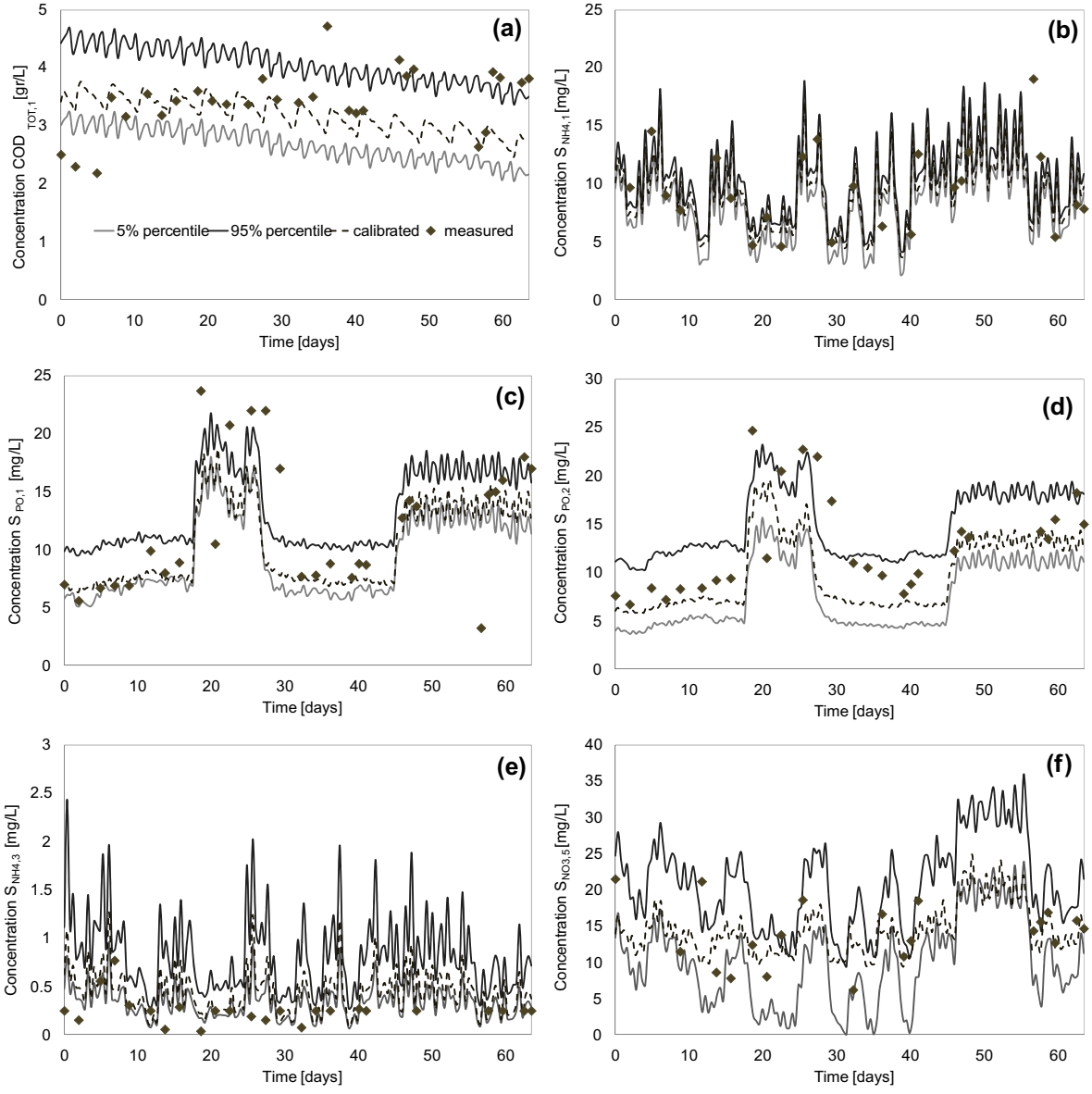

Fig. 4. Uncertainty bands, measured data, 5 and 95% percentiles for $COD_{TOT,1}$ (a), $S_{NH4,1}$ (b), $S_{PO,1}$ (c) and $S_{PO,2}$ (d), $S_{NH4,3}$ (e) and $S_{NO3,5}$ (f).

that the biological processes occurring inside the anaerobic tank are not relevant in terms of $S_{NH4,1}$ variation even during the nitrogen peak load periods. Conversely, for $S_{NH4,3}$ the high value of max_{WDTH}/$average_{WDTH}$ (3.31) indicates that the uncertainty of the model prediction varies during the simulation period suggesting that the uncertainty of factors related to the nitrification (especially of μ_{AUT} and b_{AUT}) strongly influences the model predictions in terms of $S_{NH4,3}$. Moreover, a further uncertainty for $S_{NH4,3}$ is due to the ammonification process (i.e. conversion of organic nitrogen in ammonia) that takes place in the aerobic tank.

Regarding S_{PO} (Fig. 4(c) and (d)), the results show an increasing trend of the uncertainty bands from section 1 to section 3. Such a result is confirmed by the ARIL values (0.41 and 0.64 for $S_{PO,1}$ and $S_{PO,2}$, respectively) and by the value of D_max5% and D_max95%, 5.86 and 6.77 mg/L, respectively, for $S_{PO,1}$ and 6.94 and 9.06 mg/L for $S_{PO,2}$. Indeed, these values show an increasing trend of the uncertainty from the first to the last plant section. The increase of the uncertainty

band width for $S_{PO,2}$ is most likely attributable to the key role that the factor $i_{P,BM}$ has in regulating the $S_{PO,2}$ variation due to the PAOs anoxic growth.

Indeed, as well known, under anoxic conditions, PAOs growth using nitrite and nitrate as electron acceptors and organic matter are stored under anaerobic conditions [34,39]. For $S_{NO3,5}$, despite the complexity of the involved processes, 90% of measured data lay inside the bands showing a good model (Fig. 4(f)). Moreover, the $max_{WDTH}/average_{WDTH}$ (very close to 1) shows that over the entire simulation period, the uncertainty does not change and the variations of the influent nitrogen do not influence the uncertainty of $S_{NO3,5}$. However, in terms of max_{WDTH}, D_max5% and D_max95% (12.81, 13.77 and 19.04 mg/L, respectively) the results show that $S_{NO3,5}$ is characterised by a high uncertainty as demonstrated by the wideness of the uncertainty bands. This is mainly due the uncertainty propagation from the input to the output that has an important role on the model outputs for section 5.

3.3. Implications for modellers

Results discussed in this paper show how relevant is: (1) to select both physical and biological important model factors; (2) to consider the model efficiency as reference model output; (3) to perform a plant section approach for uncertainty analysis. Regarding the point (1), as shown both during the GSA and GLUE application only by performing a comprehensive analysis of the model uncertainty (including physical and biological model factors), the modeller will be able to improve his/her knowledge and understanding of the role played by each process (physical and biological) on the effectiveness of the model predictions. Indeed, results of sensitivity and uncertainty analysis have underlined, especially in terms of total model efficiency, that the integration between physical and biological processes has a relevant role for the improvement of model predictions. Regarding the point (2), results revealed that some model factors were identified as important only on the basis of the model efficiency (e.g. F_{SA} for $COD_{TOT,1}$ or K_O and $K_{NH,A}$ for $S_{NH4,1}$). Finally, regarding the point (3) by performing the uncertainty analysis based on a plant sections approach, the modeller will be able to discriminate the contribution to the total uncertainty of each relevant process occurring inside the system. Indeed, the results show that the uncertainty propagation from the influent to the effluent has an important role for uncertainty of the last plant section (section 5). Results show that the model output uncertainty for section 5 is also affected by the uncertainty related to the model prediction of the upstream plant sections. In other words, a propagation of uncertainty as a chain from upstream to downstream takes place. Thus, from the modelling point of view, it is suggested to accurately evaluate the key source of uncertainty of the model predictions related to each plant section.

4. Conclusions

Different results were obtained for each model output and plant section. For the MLSS model outputs, factors $i_{TSS,XI}$, F_{XI} and f_{Xi} represent the key source of uncertainty. The GSA results showed a lower linearity of COD model outputs than others; nevertheless, the results are consistent with the modelled processes. For the nitrogen model outputs, the key source of uncertainty is related to the factors μ_{AUT} and b_{AUT}, these factors mainly affected the prediction in the last plant sections. For the model outputs related to the phosphorus, an increase of the uncertainty from the first to the last plant section was obtained.

Acknowledgments

This work forms part of a research project supported by grant of the Italian Ministry of Education, University and Research (MIUR) through the Research project of national interest PRIN2012 (D.M. 28 dicembre 2012 n. 957/Ric—Prot. 2012PTZAMC) entitled "Energy consumption and GreenHouse Gas (GHG) emissions in the wastewater treatment plants: a decision support system for planning and management". This study was also financially supported by MIUR within the Research project of national interest PRIN 2010-2011 (D.M. 1152/ric 27/12/2011—Prot. 2010 WLNFYZ) entitled "Emerging contaminants in air, soil, and water: from source to the marine environment".

References

[1] S.J. Judd and C. Judd, Principles and Applications of Membrane Bioreactors in Water and Wastewater Treatment, second ed., Elsevier, London, 2010.
[2] M. Henze, W. Gujer, T. Mino and M.C.M. van Loosdrecht, Activated sludge models ASM1, ASM2, ASM2d and ASM3. IWA Task Group on Mathematical Modelling for Design and Operation of Biological Wastewater treatment, IWA, London, 2000.
[3] A. Fenu, G. Guglielmi, J. Jimenez, M. Spèrandio, D. Saroj, B. Lesjean, C. Brepols, C. Thoeye, I. Nopens, Activated sludge model (ASM) based modelling of membrane bioreactor (MBR) processes: A critical review with special regard to MBR specificities, Water Res. 44(15) (2010) 4272–4294.

[4] G. Mannina, A. Cosenza, P.A. Vanrolleghem, G. Viviani, A practical protocol for calibration of nutrient removal wastewater treatment models, J. Hydroinform. 13(4) (2011) 575–595.
[5] Z. Ahmed, J. Cho, B.R. Lim, K.G. Song, K.H. Ahn, Effects of sludge retention time on membrane fouling and microbial community structure in a membrane bioreactor, J. Membr. Sci. 287 (2007) 211–218.
[6] W. Naessens, T. Maere, I. Nopens, Critical review of membrane bioreactor models—Part 1: Biokinetic and filtration models, Bioresour. Technol. 122 (2012) 95–106.
[7] M.F.R. Zuthi, W.S. Guo, H.H. Ngo, L. Nghiem, F.I. Hai, Enhanced biological phosphorus removal and its modeling for the activated sludge and membrane bioreactor processes, Bioresour. Technol. 139 (2013) 363–374.
[8] A. Zarragoitia-González, S. Schetrite, M. Alliet, U. Jáuregui-Haza, C. Albasi, Modelling of submerged membrane bioreactor: Conceptual study about link between activated slugde biokinetics, aeration and fouling process, J. Membr. Sci. 325 (2008) 612–624.
[9] L. Chen, Y. Tian, C. Cao, S. Zhang, S. Zhang, Sensitivity and uncertainty analyses of an extended ASM3-SMP model describing membrane bioreactor operation, J. Membr. Sci. 389 (2012) 99–109.
[10] A. Cosenza, G. Mannina, M.B. Neumann, G. Viviani, P.A. Vanrolleghem, Biological nitrogen and phosphorus removal in membrane bioreactors: Model development and parameter estimation, Bioproc. Biosyst. Eng. 36(4) (2013) 499–514.
[11] A. Cosenza, G. Mannina, P.A. Vanrolleghem, M.B. Neumann, Variance-based sensitivity analysis for wastewater treatment plant modelling, Sci. Tot. Environ. 470–471 (2014) 1068–1077.
[12] G. Mannina, G. Viviani, Hybrid moving bed biofilm reactors: An effective solution for upgrading a large wastewater treatment plant, Water Sci. Technol. 60(5) (2009) 1103–1116.
[13] G. Mannina, G. Viviani, Separate and combined sewer systems: A long-term modelling approach, Water Sci. Technol. 60(3) (2009) 555–565.
[14] A. Saltelli, M. Ratto, T. Andres, F. Campolongo, J. Cariboni, D. Gatelli, M. Saisana, S. Tarantola, Global Sensitivity Analysis, The Primer, John Wiley, Chichester, 2008.
[15] E. Belia, Y. Amerlinck, L. Benedetti, G. Sin, B. Johnson, P.A. Vanrolleghem, K.V. Gernaey, S. Gillot, M.B. Neumann, L. Rieger, A. Shaw, K. Villez, Wastewater treatment modelling: Dealing with uncertainties, Water Sci. Technol. 60(8) (2009) 1929–1941.
[16] H. Yuan, G. Sin, Uncertainty and sensitivity analysis of filtration models for non-Fickian transport and hyperexponential deposition, Chem. Eng. J. 168(2) (2011) 635–648.
[17] A. Robles, M.V. Ruano, J. Ribes, A. Seco, J. Ferrer, Global sensitivity analysis of a filtration model for submerged anaerobic membrane bioreactors (AnMBR), Bioresour. Technol. 158 (2014) 365–373.
[18] X. Flores-Alsina, I. Rodriguez-Roda, G. Sin, K.V. Gernaey, Uncertainty and sensitivity analysis of control strategies using the benchmark simulation model no. 1 (BSM1), Water Sci. Technol. 59(3) (2009) 491–499.
[19] G. Sin, K.V. Gernaey, M.B. Neumann, M. van Loosdrecht, W. Gujer, Global sensitivity analysis in wastewater treatment plant model applications: Prioritizing sources of uncertainty, Water Res. 45 (2011) 639–651.
[20] K.J. Beven, A.M. Binley, The future of distributed models: Model calibration and uncertainty prediction, Hydrol. Process. 6(3) (1992) 279–298.
[21] G. Mannina, Uncertainty assessment of a water quality model for ephemeral rivers using GLUE analysis, J. Environ. Eng. ASCE 137(3) (2011) 177–186.
[22] M. Ratto, S. Tarantola, A. Saltelli, Sensitivity analysis in model calibration GSA-GLUE approach, Comput. Phys. Commun. 136 (2001) 212–224.
[23] L. Vezzaro, P.S. Mikkelsen, Application of global sensitivity analysis and uncertainty quantification in dynamic modelling of micropollutants in stormwater runoff, Environ. Modell. Softw. 27–28 (2012) 40–51.
[24] T. Jiang, S. Myngheer, D.J.W. De Pauw, H. Spanjers, I. Nopens, M.D. Kennedy, G. Amy, P.A. Vanrolleghem, Modelling the production and degradation of soluble microbial products (SMP) in membrane bioreactors (MBR), Water Res. 42(20) (2008) 4955–4964.
[25] C. Lubello, S. Caffaz, R. Gori, G. Munz, A modified activated sludge model to estimate solids production at low and high solids retention time, Water Res. 43(18) (2009) 4539–4548.
[26] X.Y. Li, X.M. Wang, Modelling of membrane fouling in a submerged membrane bioreactor, J. Membr. Sci. 278 (2006) 151–161.
[27] APHA, AWWA, WEF, Standard Methods for the Examination of Water and Wastewater, Twentieth ed., American Public Health Association/American Water Works Association/Water Environment Federation, Washington, DC, 1998.
[28] G. Freni, G. Mannina, G. Viviani, Uncertainty in urban stormwater quality modelling: The effect of acceptability threshold in the GLUE methodology, Water Res. 42 (2008) 2061–2072.
[29] L.R. Iman, W.J. Conover, A distribution-free approach to inducing rank correlation among input variables, Commun. Statist. Simula. Computa. 11 (1982) 311–334.
[30] X. Jin, C.-Y. Xu, Q. Zhang, V.P. Singh, Parameter and modeling uncertainty simulated by GLUE and a formal Bayesian method for a conceptual hydrological model, J. Hydrol. 383 (2010) 147–155.
[31] G. Mannina, G. Di Bella, G. Viviani, An integrated model for biological and physical process simulation in membrane bioreactors (MBRs), J. Membrane Sci. 376 (2011) 56–69.
[32] G. Mannina, G. Di Bella, Comparing two start-up strategies for MBRs: Experimental study and mathematical modelling, Biochem. Eng. J. 68 (2012) 91–103.
[33] R. Brun, M. Kühni, H. Siegrist, W. Gujer, P. Reichert, Practical identifiability of ASM2d parameters—systematic selection and tuning of parameter subsets, Water Res. 36(16) (2002) 4113–4127.
[34] A. Cosenza, G. Mannina, P.A. Vanrolleghem, M.B. Neumann, Global sensitivity analysis in wastewater applications: A comprehensive comparison of different methods, Environ. Modell. Softw. 49 (2013) 40–52.
[35] H. Hauduc, L. Rieger, T. Ohtsuki, A. Shaw, I. Takàcs, S. Winkler, A. Héduit, P.A. Vanrolleghem, S. Gillot, Activated sludge modelling: Development and

potential use of a practical applications database, Water Sci. Technol. 63(10) (2011) 2164–2182.
[36] S.R. Weijers, P.A. Vanrolleghem, A procedure for selecting best identifiable parameters in calibrating activated sludge model no.1 to full-scale plant data, Water Sci. Technol. 36(5) (1997) 69–79.
[37] S. Kang, W. Lee, S. Chae, H. Shin, Positive roles of biofilm during the operation of membrane bioreactor for water reuse, Desalination 202(1–3) (2007) 129–134.
[38] S.T.F.C. Mortier, S. Van Hoey, K. Cierkens, K.V. Gernaey, P. Seuntjens, B. De Baets, T. De Beer, I. Nopens, A GLUE uncertainty analysis of a drying model of pharmaceutical granules, Eur. J. Pharm. Biopharm. 85(3) (2013) 984–995.
[39] G.A. Ekama, M.C. Wentzel, Denitrification kinetics in biological n and p removal activated sludge systems treating municipal wastewaters, Water Sci. Technol. 39(6) (1999) 69–77.